Magnetic Resonance Imaging 62 (2019) 38–45

Contents lists available at ScienceDirect

Magnetic Resonance Imaging

journal homepage: www.elsevier.com/locate/mri

Technical Note

# Modified look-locker inversion recovery (MOLLI) $T_1$ mapping with inversion group (IG) fitting – A method for improved precision

Marshall S. Sussman[a,b,*], Bernd J. Wintersperger[a,b]

[a] Joint Department of Medical Imaging, University Health Network, University, Toronto, Ontario, Canada
[b] Department of Medical Imaging, University of Toronto, Toronto, Ontario, Canada

ARTICLE INFO

*Keywords:*
MOLLI
$T_1$
MRI
Cardiac
Look-locker
Inversion group

ABSTRACT

MOLLI-based T1 mapping has been applied to a variety of cardiac pathologies. However, conventional MOLLI's requirement for rest periods between inversion groups increases scan time, and limits the choice of inversion groups. The recently developed inversion group (IG) fitting technique eliminates the rest period requirement, and permits complete flexibility of inversion groups. However, a limitation is that its T1 maps have low precision – up to 30% poorer than conventional 3-parameter methods. In the original IG method, T1 maps were derived from the first inversion group only. In the present study, a technique is presented which utilize data from all inversion groups to generate T1 maps. It is hypothesized this "composite-IG" fitting method will provided improved prevision over conventional-IG T1 mapping methods. Simulations, phantom, and in vivo experiments on nine clinical cardiac patients (congenital heart disease, ischemic- and non-ischemic cardiomyopathy) were performed. Imaging was performed on a 1.5 T Siemens scanner. Myocardial T1 mapping precision and reproducibility were calculated for conventional-IG, composite-IG, and 3-parameter techniques. Precision and reproducibility between the techniques was compared using the Wilcoxon Signed Rank test. Statistical significance was set at the 95% confidence level, with the Bonferroni correction for multiple comparisons employed. Composite-IG improves precision by 16–38% over conventional-IG ($p < 0.01$). Composite-IG T1 maps provided up to 5% better precision than 3-parameter fits ($p < 0.01$). Composite-IG had better reproducibility than conventional-IG ($p < 0.01$). However, there was no significant difference between composite-IG and conventional 5(3)3 3-parameter reproducibility.

## 1. Introduction

Quantitative $T_1$ mapping may be used for characterizing cardiac pathology [1–5]. In diseases with large, focal lesions (e.g. myocardial infarction), changes in $T_1$ (or derived values, such as ECV [6]) may be quite large [7]. In these cases, discrimination of pathology is typically unambiguous. However, with more subtle, diffuse pathology (e.g. cardiomyopathy), $T_1$ changes may be less prominent [8–11]. To accurately detect changes associated with subtle abnormalities, it must be possible to distinguish changes in $T_1$ due to pathology, from changes caused by artifacts and/or noise.

One technique for cardiac $T_1$ mapping is modified look-locker inversion recovery (MOLLI) [12]. In this technique, a $180^0$ inversion pulse is applied after a specified delay following the cardiac trigger. A balanced SSFP readout then acquires data for the first inversion time (TI). Balanced SSFP readouts on subsequent cardiac cycles may be used to acquire additional inversion times. All TI times collected in this manner constitute an "inversion group". A rest period, typically consisting of three or more cardiac cycles, is then used to allow the magnetization to recover back to equilibrium. The process is repeated one or more times to acquire additional inversion groups.

Rest periods are necessary to ensure that data from the different inversion groups follow the same recovery curve [13]. Unfortunately, they lengthen scan time. This makes it more challenging for patients to hold their breath. In turn, this could lead to increased motion artifacts, and potentially large errors in $T_1$ [14,15]. Additionally, rest periods restrict the amount and type of inversion groups that can be acquired in a given time.

Recently, our group introduced a new method for $T_1$-fitting of MOLLI data called inversion group (IG) fitting [16]. Its main advantage

*Abbreviations:* $\Delta_i$, ratio between the longitudinal magnetization following the $i^{th}$ inversion pulse and the fully relaxed equilibrium (i.e. $M_0$) magnetization

* Corresponding author at: Joint Department of Medical Imaging, University Health Network, 585 University Avenue, Room NUW-1-141D, Toronto, Ontario M5G 2N2, Canada.
*E-mail addresses:* marshall.sussman@utoronto.ca (M.S. Sussman), Bernd.Wintersperger@uhn.ca (B.J. Wintersperger).

https://doi.org/10.1016/j.mri.2019.06.002
Received 6 December 2018; Received in revised form 31 May 2019; Accepted 2 June 2019

is that it does not require rest periods. However, the utility of this technique was tempered somewhat by the relatively low precision of the resulting $T_1$ maps. In this paper, we present a technique for improving the precision of IG fitting.

## 2. Materials and methods

### 2.1. Theory

In conventional MOLLI, a 3-parameter function is used to model the signal ($S$):

$$S(TI) = A - Be^{-\frac{TI}{T_1^*}} \tag{1}$$

where $T_1^*$ is the "apparent" longitudinal relaxation time. It is related to the true relaxation time ($T_1$) by [17]:

$$T_1 = T_1^* \bullet \left(\frac{B}{A} - 1\right) \tag{2}$$

Eq. (1) is valid provided that rest periods are used in between inversion groups to ensure full magnetization recovery. If full recovery does not occur, systematic errors are introduced into the $T_1$ values [16].

In IG-MOLLI, the rest period requirement is eliminated through a function that is piecewise continuous over the $n$ inversion groups:

$$S_i(A, B_1, ..., B_i, T_1^*; TI) \equiv A - B_i e^{-\frac{TI}{T_1^*}};\ i = 1,\ ..., n \tag{3}$$

Note that this function employs one "$A$" and one "$T_1^*$" parameter, but $n$ "$B_i$" parameters.

$T_1$ may be derived as [13,16]:

$$T_1^i = T_1^* \bullet \left(\frac{B_i}{A} - 1\right)/\Delta_i;\ i = 1,\ ..., n \tag{4}$$

where $\Delta_i$ is the ratio between the longitudinal magnetization following the $i^{th}$ inversion pulse and the fully relaxed equilibrium (i.e. $M_0$) magnetization. (Note that this definition of $\Delta_i$ differs slightly from the "inversion factor" interpretation used in Ref. [13]. See the paper by Kampf et al. [18] for a more detailed physical interpretation of this quantity).

Since all $T_1$ values calculated via Eq. (4) should be the same:

$$T_1^1 = T_1^2 = ... = T_1^n \equiv T_1 \tag{5}$$

it is in theory possible to derive $T_1$ from any inversion group. Unfortunately, only $\Delta_1$ is known a priori. It is equal to unity (ignoring non-idealities in the adiabatic $180^0$ pulse, which may be corrected afterwards with a scalar multiplication [13]), For this reason, in our previous work [16], Eq. (4) was applied to the first inversion group only. For the remainder of this paper, we will refer to this technique as "single-IG MOLLI". Its drawback is that only a portion of the available data is used. In this paper, we describe a method for estimating $\Delta_i$, and therefore ${T_1}^i$, from all inversion groups. All ${T_1}^i$'s may then be combined into a single composite $T_1$ estimate. Since this approach utilizes additional data relative to the single-IG method, we hypothesize that improved precision will be achieved. We will refer to this latter technique as "composite-IG MOLLI".

The algorithm begins with the calculation of *uncorrected* $T_1$ estimates:

$$T_{1_{uncorr}}^i(x,y) \equiv T_1^*(x,y) \bullet \left(\frac{B_i(x,y)}{A(x,y)} - 1\right);\ i = 1,\ ..., n \tag{6}$$

Using Eqs. (4) and (5) together with the fact that $\Delta_1 = 1$, the following expression may be derived:

$$\Delta_i(x,y) = \frac{T_{1_{uncorr}}^i(x,y)}{T_{1_{uncorr}}^1(x,y)};\ i = 1,\ ..., n \tag{7}$$

In theory, it may be supposed that we could simply insert Eq. (7) into Eq. (4) to calculate ${T_1}^i$ for all inversion groups. However, because the same data is used to calculate both ${T_1}^i$ and $\Delta_i$, all ${T_1}^i$'s would reduce tautologically to ${T_1}^1$. Additionally, the noise of the $\Delta_i$ estimates will be at least as large as ${T_1}_{uncorr}^{\ i}$. This will lead to a significant increase in the noise of the ${T_1}^i$ estimates calculated via Eq. (4). To address both problems, one possibility could be to calculate $\Delta_i$ at each position $(x,y)$ as an average over a set of neighbouring pixels:

$$\Delta_i(x,y) = \frac{\sum_{j \in Set\ of\ Neighbouring\ Pixels\ to\ (x,y)} \{T_{1_{uncorr}}^i(x,y)\}}{\sum_{j \in Set\ of\ Neighbouring\ Pixels\ to\ (x,y)} \{T_{1_{uncorr}}^1(x,y)\}};\ i = 1,\ ..., n \tag{8}$$

The disadvantage with this "unconstrained" averaging is that adjacent pixels may not necessarily have the same $\Delta_i$. This could introduce bias and/or blurring into the $\Delta_i$ estimates. Therefore, we instead perform constrained averaging. Only pixels that are similar will be averaged. At each location $(x,y)$, similar pixels are defined (Fig. 1) as those that:

i) Are within a specified distance of the location $(x,y)$
ii) Have an uncorrected $T_1$ value within a specified percentage of ${T_1}_{uncorr}^{\ 1}(x,y)$.

It was found that a distance tolerance of 7 × 7 pixels and a $T_1$ tolerance of 5% optimizes precision.

The $\Delta_i$'s are then calculated using a modified version of Eq. (8):

$$\Delta_i(x,y) = \frac{\sum_{j \in Set\ of\ Similar\ Pixels\ to\ (x,y)} \{T_{1_{uncorr}}^i(x,y)\}}{\sum_{j \in Set\ of\ Simiar\ Pixels\ to\ (x,y)} \{T_{1_{uncorr}}^1(x,y)\}};\ i = 1,\ ..., n \tag{9}$$

The $\Delta_i$'s are inserted into Eq. (4) to derive $T_1$ estimates from each inversion group. Finally, $T_1$ estimates are combined in a weighted sum

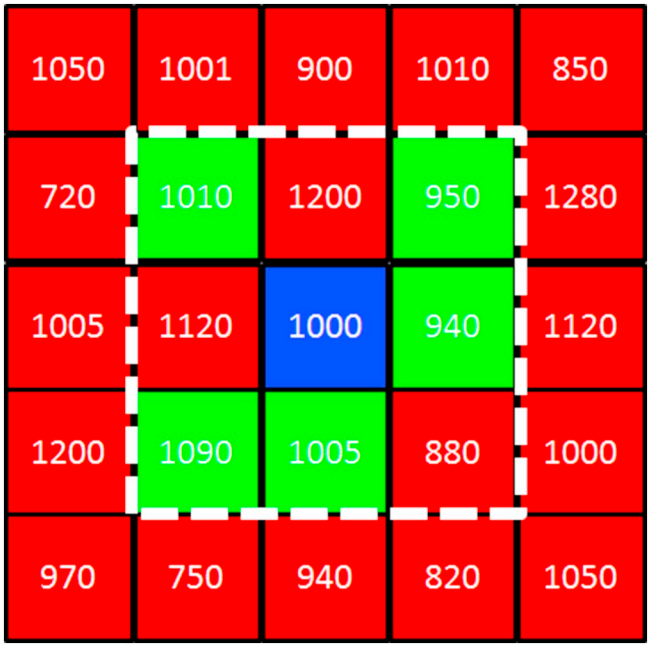


**Fig. 1.** Pixel selection algorithm. Each element of the grid represents a pixel. The number in the centre of each pixel is its $T_1$ value. In this example, pixels will be selected that are similar to the blue pixel in the centre, which has a $T_1$ value of 1000 ms. A distance tolerance of 3 × 3 pixels around the blue pixel will be used (dashed white line). Only pixels inside of this line satisfy the distance tolerance. The $T_1$ tolerance for this example will be those pixels with a $T_1$ value within 10% of the blue pixel $T_1$ (i.e. $T_1$ between 900 and 1100 ms). The green pixels satisfy both tolerances, while the red pixels violate at least one of the tolerances. The green pixels therefore represent the set of pixels that are similar to the blue one. After repeating this process at every location, a set of similar pixels will be associated with each pixel in the image. (For interpretation of the references to colour in this figure legend, the reader is referred to the web version of this article.)

to produce a composite $T_1$ estimate:

$$T_1^{composite} = \sum_{k=1}^{n} w_k(x,y) \bullet T_1^k(x,y) \Big/ \sum_{k=1}^{n} w_k(x,y) \quad (10)$$

For optimal SNR [19], the weighting factor for inversion group $k$ at position $(x,y)$ is chosen to be the inverse variance in $T_1{}^k(x,y)$ over the set of similar pixels at location $(x,y)$.

### 2.2. Experimental overview

Simulation, phantom, and in vivo experiments were performed to validate the composite-IG technique. For all experiments, four MOLLI acquisition schemes were used. These were labelled as "$w(x)y$"; where non-bracketed numbers indicate an inversion group, and bracketed numbers indicate a rest period (in heartbeats). The first scheme, 5(3)3, consisted of an inversion group with five TI's, a three-heartbeat rest period, and finally a second group with three TI's. This is a commonly used scheme for pre-contrast $T_1$ measurements [14]. The long rest period typically allows full magnetization recovery back to equilibrium. The second scheme, 5(0)3, eliminates the rest period. It thus acquires the same amount of data as the first scheme (i.e. 8 TI's), but in three less heartbeats than 5(3)3. This scheme therefore has a 27% shorter scan time. The third scheme was 5(0)3(0)3. It acquires more data (11 TI's) in the same scan time as 5(3)3. The last acquisition scheme was 1(0)2(0)3(0)5. This was chosen because it strongly emphasizes incomplete magnetization recovery due to the short length of the early inversion groups, as well as the absence of rest periods. It therefore provides an extreme test for the algorithm. Other relevant acquisition parameters were matrix = 256 × 192, GRAPPA acceleration factor = 2, number of reference lines = 32, percent phase FOV = 75%, flip angle = $35^0$, TR = 2.7 ms, and TE = 1.2 ms. The first TI was 120 ms, and subsequent TI groupings were incremented by 80 ms.

All analysis was performed in Matlab (release 2013b, The MathWorks, Natick, MA).

### 2.3. Simulations

A Monte Carlo simulation using 5000 trials of the Bloch Equations [20] was performed. The fully relaxed (i.e. $M_0$) SNR was set to 100. This yielded a maximum SNR of about 20 in the resulting MOLLI images. $T_1$ was varied from 600 to 1200 ms, in steps of 100 ms. A $T_2$ value of 50 ms, and an RR interval of 1000 ms were used. IG fits (Eq. (3)) were performed using both single- and composite-IG methods. Conventional 3-parameter fitting (Eq. (1)) was also applied to the 5(3)3 data. The accuracy of the fitting methods was assessed by comparing the fitted and true $T_1$ values. The precision was calculated as the coefficient-of-variance (COV) over the simulation trials.

For the composite-IG method, the $\Delta_i$'s were calculated in two different ways: First, they were calculated using the noisy data. In vivo, this would correspond to the case where no pixel selection is used (i.e. Eq. (7), where the $\Delta_i$'s are calculated from single noisy pixels). In the second case, $\Delta_i$'s were calculated from noiseless data. In vivo, this would correspond to the case of perfect pixel selection (i.e. Eq. (9), where $n \rightarrow \infty$, and no systematic errors (e.g. blurring, bias) are introduced by the pixel selection process). These two cases represent the extrema of precision that are achievable by the composite-IG technique.

### 2.4. Phantom experiments

A phantom was constructed using $MnCl_2$-doped agar. Chemical concentrations were adjusted to achieve a $T_1$ value of 942 ms and a $T_2$ value of 40 ms. The phantom was scanned with 5(3)3, 5(0)3, 5(0)3(0)3, and 1(0)2(0)3(0)5 acquisitions. For each acquisition scheme, three separate scans were performed. Pixelwise $T_1$ maps were calculated using single- and composite-IG MOLLI. A 3-parameter fit was also performed on the 5(3)3 data.

Precision was first assessed by calculating the standard deviation in $T_1$ over the three repeated acquisitions. Unfortunately, while this approach is useful in the present phantom case, it would be difficult to apply in vivo due to motion and/or artifacts between the repeated acquisitions. Therefore, a second method for assessing precision that is more appropriate for in vivo applications was also tested. The method of Kellman et al. [14] calculates precision through a propagation-of-errors analysis of the $T_1$-fitting functions. It only requires a single acquisition. We have previously validated the equality of these two techniques in the case of single-IG MOLLI [16]. In the present study, we further validate the equality of the two precision techniques for composite-IG MOLLI. This was accomplished through a *t*-test.

The effectiveness of the composite-IG method for improving $T_1$ mapping precision was assessed in two different ways: First, the precision of single- and composite-IG $T_1$ maps were compared. Second, the precision of composite-IG and the reference 3-parameter 5(3)3 $T_1$ maps were assessed. In both cases, *t*-tests were used to perform the comparison. Statistical significance was set at the 95% confidence level.

### 2.5. In vivo experiments

Nine clinical cardiac patients (congenital heart disease, ischemic- and non-ischemic cardiomyopathy) were scanned. The mean RR-interval was 880 ± 225 ms (range: 523-1255 ms). The study protocol was approved by the institutional research ethics board, and all patients provided written informed consent. Experiments were performed on a 1.5 T scanner (Magnetom Avanto fit, Siemens Healthcare Erlangen, Germany).

All patients were scanned with 5(3)3, 5(0)3, 5(0)3(0)3, and 1(0)2(0)3(0)5. For each acquisition scheme, three separate scans in a mid-ventricular slice were performed.

Following motion correction [21], pixelwise $T_1$ maps were calculated using single- and composite-IG MOLLI. A 3-parameter fit was also performed on the 5(3)3 data. Myocardial ROIs were drawn on each $T_1$ map, and used for all subsequent analyses. To avoid the confounding effects of partial volumes and/or artifacts, ROIs were drawn conservatively to avoid borders and any obvious artefactual areas.

The objective of the pixel selection algorithm is to improve the SNR of the $\Delta_i$ estimates. However, averaging together multiple pixels (even in a constrained manner, as is done presently) could cause artifacts (e.g. bias, blurring, etc.). In a given pixel, this could lead to the $\Delta_i$'s calculated through pixel selection deviating from the $\Delta_i$ values that would have been obtained without averaging. To assess the significance of this problem, the $\Delta_i$'s derived from the pixel selection algorithm (i.e. Eq. (9)) were compared to the non-averaged $\Delta_i$'s calculated from Eq. (7) with a *t-test*.

The accuracy of composite-IG MOLLI $T_1$ values was calculated in two different ways: First, the mean discrepancy over the myocardial ROI relative to the single-IG $T_1$ values was assessed. (Note that the accuracy of the single-IG MOLLI $T_1$ values has already been established previously [16], so it was assumed to provide a reference standard). A Wilcoxon Signed Rank test was used to test for non-zero discrepancy. Second, the myocardial $T_1$ values of the composite-IG fits were compared to the conventional 5(3)3 3-paramaeter fit. An ANOVA test was used to perform the comparison.

The precision of the in vivo $T_1$ maps was calculated using the method of Kellman et al. [14] (that was discussed and validated in the Phantom section). Two precision tests were performed: First, the precision of single- and composite-IG techniques was compared. Second, the precision of composite-IG $T_1$ values was compared to the 3-parameter data. Wilcoxon Signed Rank tests were used to perform the comparisons.

Reproducibility was calculated as the standard deviation across the three repeated acquisitions within the myocardial ROI. Assessment was performed in a similar manner to precision.

Statistical significance was set at the 95% confidence level, with the

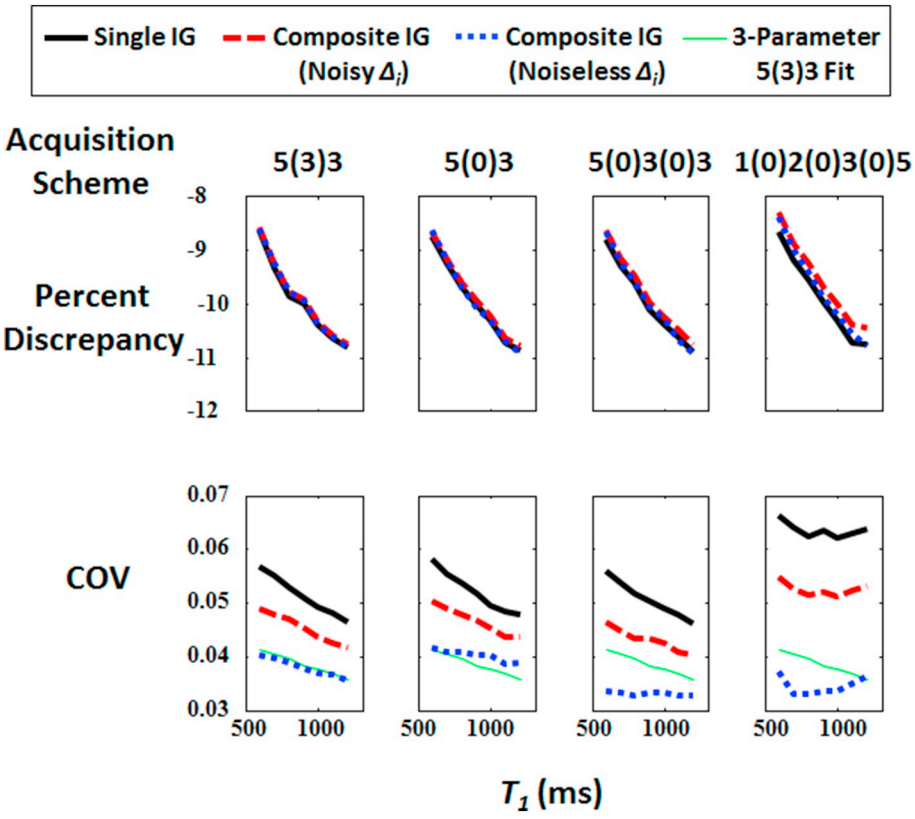


**Fig. 2.** Simulation results for single- and composite IG-MOLLI (using both noisy and noiseless $\Delta_i$ calculations for the latter). The top half of the figure plots the percent discrepancy in the fitted $T_1$ relative to the true $T_1$ value. The bottom half of the figure plots the coefficient of variation (COV = precision/True $T_1$). The COV of the conventional 3-parameter fit for the 5(3)3 acquisition is also plotted.

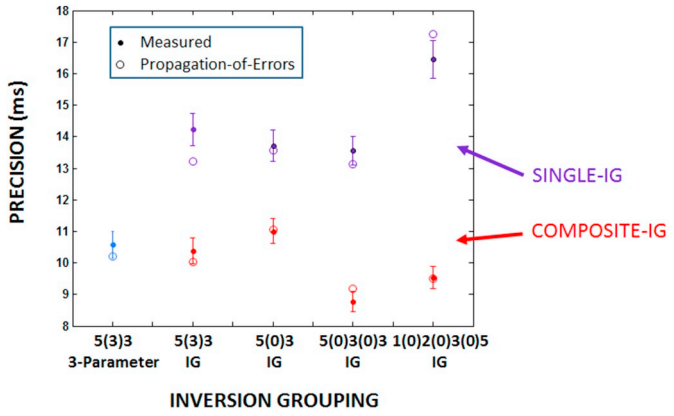


**Fig. 3.** Precision results for the phantom experiment. The solid circles represent the mean precision measured over the phantom ROI. The precision was calculated pixelwise as the standard deviation across three repeated trials. The error bars represent the standard error over the ROI. The open circles represent the precision calculated through the propagation-of-errors technique.

Bonferroni correction for multiple comparisons employed.

## 3. Results

### 3.1. Simulations

The top half of Fig. 2 plots the percent discrepancy between fitted and true $T_1$ values for the different MOLLI acquisition schemes. Note that the global systematic underestimation of the true $T_1$ value is a well-known issue inherent in conventional MOLLI methods [12,15]. It is not pertinent to the current study. What is of interest is that the single- and composite-IG discrepancies are virtually identical. This indicates that composite-IG MOLLI is not introducing systematic errors into the $T_1$ maps. The bottom half of Fig. 1 plots precision. As expected [16], single-IG MOLLI has relatively poorer precision. The precision of composite-IG MOLLI, on the other hand, is significantly improved. However, the improvement in precision depends on the noise level in the $\Delta_i$'s. In the case of noiseless $\Delta_i$ calculations, the 5(0)3(0)3 and 1(0)2(0)3(0)5 composite-IG $T_1$ precisions are actually better than the conventional 5(3)3 3-parameter precision.

**Table 1**
In vivo $\Delta_i$ results: Listed values represent the discrepancy between myocardial $\Delta_i$ values calculated through pixel selection (using constrained averaging) and $\Delta_i$ values calculated without averaging.

| Inversion grouping | Percent discrepancy | *p*-Value |
|---|---|---|
| 5(3)3 | −0.20 ± 0.26% | $< 10^{-4}$ |
| 5(0)3 | −0.07 ± 0.47% | $< 10^{-4}$ |
| 5(0)3(0)3 | 0.01 ± 0.52% | $< 10^{-4}$ |
| 1(0)2(0)3(0)5 | −0.76 ± 0.83% | $< 10^{-4}$ |

**Table 2**
In vivo $T_1$ accuracy results. Listed data represents the discrepancy between single- and composite-IG myocardial $T_1$ values. The "*" indicates statistical significance at the 95% confidence level.

| Inversion grouping | Discrepancy (ms) | Discrepancy (%) | *p*-Value |
|---|---|---|---|
| 5(3)3 | −0.4 ± 0.8 | −0.04 ± 0.08% | 0.027* |
| 5(0)3 | −0.4 ± 1.2 | −0.04 ± 0.1% | 0.82 |
| 5(0)3(0)3 | 0.8 ± 3.2 | 0.09 ± 0.1% | 0.65 |
| 1(0)2(0)3(0)5 | −5.7 ± 4.5 | −0.6 ± 0.5% | 0.04* |

### 3.2. Phantom experiment

Fig. 3 plots the precision results for the phantom experiment. There was no significant difference in the precision measured through repeated trials, and the precision calculated through the propagation-of-errors technique ($p > 0.05$ in all cases). This (now validated)

**Table 3**
In vivo $T_1$ precision results. Non-bracketed data represents the standard deviation and bracketed data represents the coefficient-of-variation (=standard deviation/$T_1$).

| Inversion grouping | Single-IG | Composite-IG | 3-Parameter |
|---|---|---|---|
| 5(3)3 | 21.1 ± 6.3 ms (0.0217 ± 0.0068) | 16.4 ± 5.1 ms (0.0169 ± 0.0055) | 16.0 ± 5.1 ms (0.0164 ± 0.0053) |
| 5(0)3 | 21.2 ± 6.4 ms (0.0222 ± 0.0070) | 17.9 ± 5.5 ms (0.0186 ± 0.0060) | – |
| 5(0)3(0)3 | 20.0 ± 5.7 ms (0.0211 ± 0.0066) | 15.2 ± 4.9 ms (0.0160 ± 0.0053) | – |
| 1(0)2(0)3(0)5 | 26.2 ± 7.7 ms (0.0275 ± 0.0083) | 16.3 ± 4.9 ms (0.0169 ± 0.0055) | – |

propagation-of-errors technique will be used subsequently for the in vivo experiments – where motion, artifacts, and biologic variation in $T_1$ make it challenging to asses precision through repeated acquisitions and/or measurements over an ROI.

The precision of the composite-IG $T_1$ maps was significantly better than the single-IG $T_1$ maps in all cases ($p < 0.001$). This formally validates the improved precision provided by the composite-IG technique.

The precision of the 5(3)3, 5(0)3, and 1(0)2(0)3(0)5 $T_1$ maps were equivalent to the precision of the 5(3)3 3-parameter $T_1$ maps ($p > 0.06$ in all cases). The 5(0)3(0)3 $T_1$ maps were significantly better ($p = 0.001$). This demonstrates that composite-IG is capable of providing $T_1$ maps that have equal or better precision than the conventional 3-parameter reference method.

### 3.3. In vivo experiment

Table 1 lists the discrepancy between $\Delta_i$'s derived from the pixel selection algorithm (using constrained averaging) and $\Delta_i$'s derived without averaging. The discrepancy is extremely small for all inversion groups (< 1%). None of the discrepancies are statistically significant.

The in vivo $T_1$ accuracy results are listed in Table 2. Only the 5(3)3 and 1(0)2(0)3(0)5 discrepancies are statistically significant. However, all discrepancies are extremely small in absolute (< 6 ms) and percentage (< 0.6%) terms. The mean myocardial $T_1$ value of the 5(3)3 3-parameter fits was 1019 ± 38 ms. This was found to be not significantly different than any of the myocardial composite-IG $T_1$ data.

Table 3 lists the in vivo $T_1$ precision results. Composite-IG improves the precision by 16–38% over single-IG. The improvement is statistically significant ($p < 0.01$ in all cases). Table 3 also lists the in vivo precision results for the conventional 3-parameter 5(3)3 fits. The single-IG MOLLI precision is much worse than the 5(3)3 3-parameter fits for all MOLLI acquisition schemes – almost 64% poorer in the case of 1(0)2(0)3(0)5. This difference was statistically significant ($p < 0.01$ in all cases). However, a dramatic improvement is observed for composite-IG MOLLI. The precision of the 5(3)3 composite $T_1$ maps are only 2% poorer than the 3-parameter $T_1$ maps ($p < 0.01$), while the 5(0)3 $T_1$ maps are 11% poorer ($p < 0.01$). The 5(0)3(0)3 $T_1$ maps have a 5% better precision, ($p < 0.01$), while the 1(0)2(0)3(0)5 $T_1$ maps are equivalent ($p = 0.13$) to the 5(3)3 3-parameter maps.

**Table 4**
In vivo $T_1$ reproducibility results. Non-bracketed data represents the standard deviation and bracketed data represents the coefficient-of-variation (=standard deviation/$T_1$).

| Inversion grouping | Single-IG | Composite-IG | 3-Parameter |
|---|---|---|---|
| 5(3)3 | 34.0 ± 7.2 ms (0.0351 ± 0.0079) | 30.5 ± 6.3 ms (0.0314 ± 0.0068) | 30.1 ± 5.1 ms (0.0309 ± 0.0057) |
| 5(0)3 | 39.2 ± 9.2 ms (0.0410 ± 0.0109) | 34.5 ± 7.0 ms (0.0361 ± 0.0086) | – |
| 5(0)3(0)3 | 39.6 ± 4.1 ms (0.0420 ± 0.0051) | 33.1 ± 4.4 ms (0.0349 ± 0.0047) | – |
| 1(0)2(0)3(0)5 | 45.1 ± 13.2 ms (0.0469 ± 0.0134) | 33.0 ± 9.3 ms (0.0343 ± 0.0096) | – |

Table 4 lists the in vivo $T_1$ reproducibility results. Composite-IG is significantly more reproducible than single-IG ($p < 0.01$ in all cases). There was no significant difference between composite-IG and the conventional 5(3)3 3-parameter reproducibility ($p = 0.61$, 0.06, 0.26, 0.32 for 5(3)3, 5(0)3, 5(0)3(0)3, and 1(0)2(0)3(0)5 respectively).

Fig. 4 illustrates examples of $\Delta_i$ maps (i.e. ratio between the longitudinal magnetization following the $i^{th}$ inversion pulse, and the fully relaxed equilibrium magnetization). For 5(3)3, with nearly full recovery during the rest period, the $\Delta_i$ map is close to unity. For 1(0)2(0)3(0)5, with incomplete recovery due to lack of rest periods, the $\Delta_i$ maps are less than unity. The previous $\Delta_i$ maps were calculated using the pixel selection algorithm (i.e. constrained averaging). For comparison, Fig. 4 also plots $\Delta_i$ maps calculated without averaging. The SNR improvement provided by pixel selection is apparent. Furthermore, there are no obvious artifacts or blurring in the averaged $\Delta_i$ maps compared to the non-averaged ones.

Fig. 5 illustrates an in vivo example with all of the different acquisition schemes and fitting types. A narrow colourmap is used to highlight differences in accuracy or precision within the myocardium. For the 3-parameter $T_1$ maps, there is significant variability in the acquisitions schemes without a rest period due to the inadequacy of the fitting model (Eq. (1)). In contrast, all IG MOLLI $T_1$ maps are very consistent. In the case of single-IG MOLLI, this consistency has been noted previously [16]. However, it is now seen that composite-IG MOLLI maintains this consistency. Although improvement in precision between single- and composite-IG techniques can be observed for all inversion groupings, it is most easily appreciated in the 1(0)2(0)3(0)5 case.

A second in vivo example is shown in Fig. 6. The top row uses a narrow colourmap to highlight the myocardium. The bottom row uses a broad colourmap to provide an indication of the effectiveness of the composite-IG method over the full range of $T_1$'s. The strong similarity between $T_1$ maps generated by 3-parameter and IG methods illustrates that IG MOLLI does not introduce systematic errors over a broad range of $T_1$'s.

## 4. Discussion

Our previous study [16] demonstrated that single-IG MOLLI provides accurate $T_1$ measurements independent of the specific MOLLI acquisition schemes and/or presence/absence of rest periods. However, the drawback of this technique was relatively poor precision. In the present study, a technique for improving the precision and reproducibility of IG fitting has been validated. This was accomplished by utilizing all of the available MOLLI data.

One potential drawback of the composite-IG technique is the use of averaging in the pixel selection algorithm. Averaging could cause artifacts (e.g. bias, blurring, etc.). However, we have established that $\Delta_i$'s derived from pixel selection are statistically equal to $\Delta_i$'s calculated without averaging. To illustrate this point graphically, note that there are no obvious signs of blurring or artifacts when comparing the averaged to non-averaged $\Delta_i$ maps in Fig. 4. To further support the validity of the pixel selection algorithm, recall that the discrepancy between single- (calculated without pixel selection) and composite-IG $T_1$ values (which utilizes pixel selection) was extremely small (0.04–0.6% or 0.4–5.7 ms).

The fact that the pixel selection produces minimal errors is likely due to two reasons: First, the averaging operation is constrained – only pixels that fall within a specified $T_1$ are included in the average. Constrained averaging therefore does not operate as a pure low-pass filter. Second, the constrained averaging operation is only applied to the $\Delta_i$ calculations (Eq. (9)). These $\Delta_i$'s are then combined with *non-averaged* $T_1^*$, $A$, and $B_i$ parameters to produce corrected $T_1$ estimates

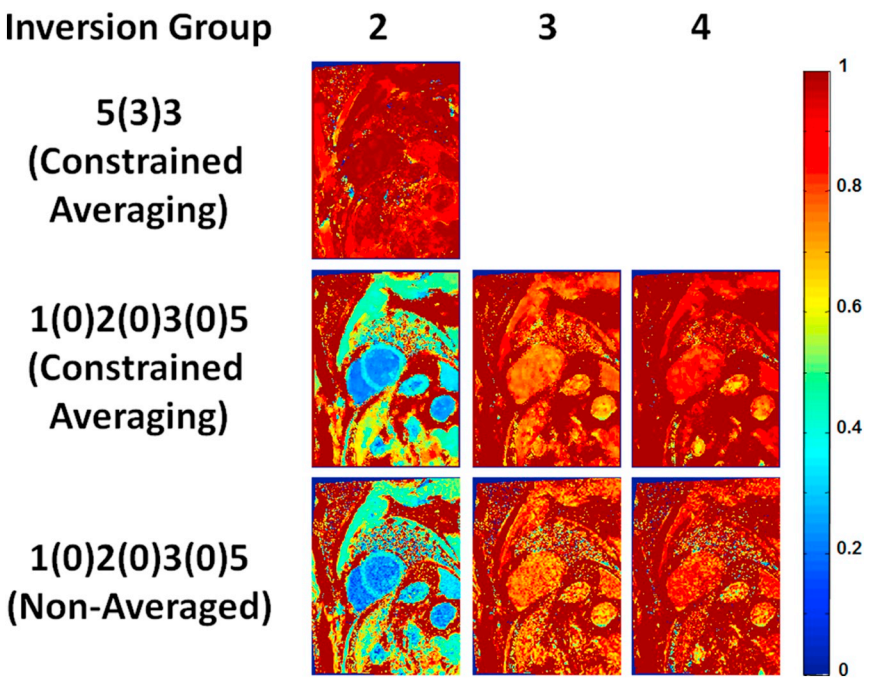


**Fig. 4.** $\Delta_i$ values for 5(3)3 and 1(0)2(0)3(0)5 MOLLI acquisition schemes. $\Delta_i$'s for the first inversion group are not shown since they are by definition unity everywhere. The upper two rows were calculated using the pixel selection algorithm (i.e. constrained averaging). The bottom row represents $\Delta_i$ values calculated on single pixels (i.e. without pixel selection or averaging).

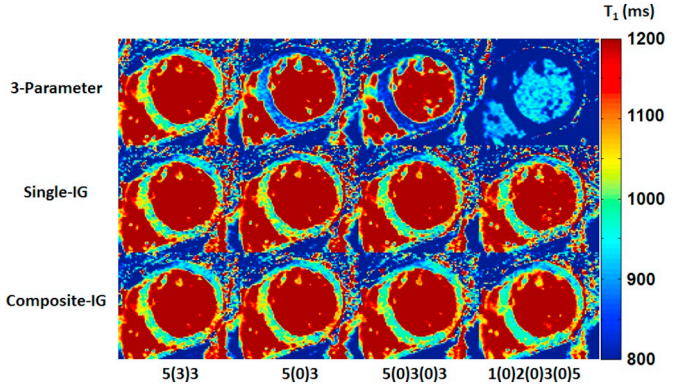


**Fig. 5.** In vivo comparison of 3-parameter, single-, and composite-IG $T_1$ maps for 5(3)3, 5(0)3, 5(0)3(0)3, and 1(0)2(0)3(0)5 MOLLI acquisition schemes. A narrow colormap window is used to highlight the myocardium.

(Eq. (4)). On the other hand, there is likely still room for improvement in the $\Delta_i$ calculations. In particular, note that the improvement in precision observed in vivo was not quite as large as predicted by simulation. For example, simulation predicted that the composite-IG 5(0)3(0)3 precision should be about 12% better than the 5(3)3 3-parameter precision if the pixel selection algorithm were perfect. However, only a 5% improvement was seen in vivo.

The most immediate application of the composite-IG technique is likely for shortening scan time. For example, by eliminating the rest period, the 5(0)3 acquisition was ~27% shorter than the conventional 5(3)3 method, while maintaining reasonable precision. This is likely to be of particular relevance in cardiac patient populations, where artifacts caused by inadequate breath holds may lead to large errors in $T_1$ [14,15]. Another potential application of composite-IG could be to achieve improved precision over conventional methods. For example, the 5(0)3(0)3 acquisition achieved a ~5% better precision than the 5(3)3 3-parameter scan. This was accomplished by acquiring additional data in the time that would normally be occupied by the rest period. In the future, it may be possible to achieve even better precision with a more systematic optimization of inversion groups [22]. However, it should be reiterated that improvements in the $\Delta_i$ calculations may also be acquired in order to fully realize the expected improvement in precision.

A recent study by Shao et al. [23] compared the performance of single-IG, 3-parameter, and two Bloch Equation-based $T_1$ mapping techniques [24]. They found that 3-parameter fitting was the best, while single-IG was the worst in terms of precision. As shown in the present study, the new composite-IG technique can now achieve a precision similar to (or, in some cases, better) than 3-parameter fitting. However, the Bloch Equations-based techniques were more accurate, and had less sensitivity to $T_2$ and flip angle variations than both single-IG and 3-parameter fitting. The composite-IG technique will not improve upon either of these latter results. On the other hand, recent work by Kampf et al. [18] has suggested some possible strategies for mitigating these issues.

The present study was performed at 1.5 T. However, the advantages of the composite-IG technique may be even more pronounced at higher field strengths. This is due to the fact that $T_1$ times increase with field strength. As a result, longer rest periods may be required for conventional 3-parameter fitting techniques to achieve full relaxation between inversion groupings. This would further reduce their efficiency. On the other hand, the composite-IG technique could still acquire data throughout (i.e. with no rest periods).

A study by Roujol et al. [25] compared the performance of 3-parameter MOLLI to other cardiac $T_1$ mapping techniques. They demonstrated that the main advantage of MOLLI was its superior precision – 70% better than SAPPHIRE [26], and 118% better than SASHA [27]. On the other hand, SAPPHIRE and SASHA had better accuracy. Single-IG fitting MOLLI can reduce scan time compared to 3-parameter MOLLI. However, its ~30% reduced precision partially erodes the overall precision advantage of MOLLI. With composite-IG fitting, reduced scan time may be achieved with only a ~10% precision loss relative to 3-parameter fitting – substantially better than SAPPHIRE or SASHA. Alternatively, instead of reduced scan time, composite IG-fitting may be used to further improve the precision advantage of MOLLI (as discussed in the previous paragraph) over the other techniques. Another competing cardiac $T_1$ mapping technique is shMOLLI [28]. Roujol et al.'s study demonstrated that the precision of shMOLLI is about 40% poorer than MOLLI. The precision of the single-IG technique is therefore superior to this. The composite-IG provides developed in this study provides even better precision performance. It should be

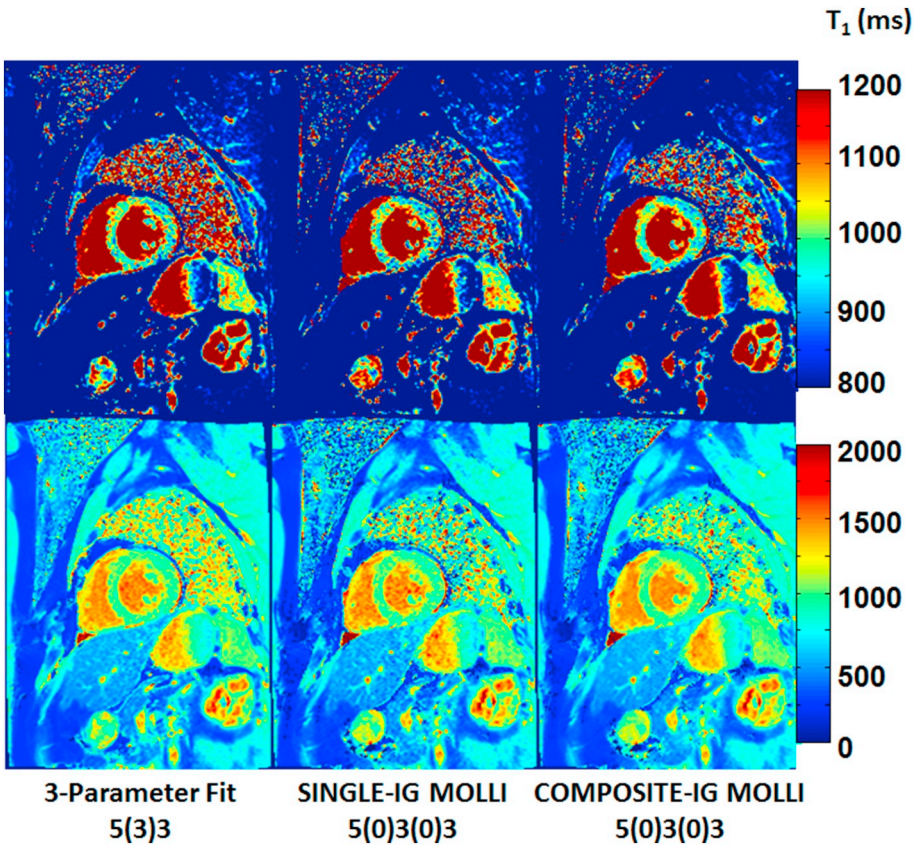


**Fig. 6.** In vivo $T_1$ map comparison of a 3-parameter 5(3)3 MOLLI acquisition scheme to single- and composite-IG 5(0)3(0)3. The top row uses a narrow colourmap to highlight differences in precision within the myocardium. The bottom row uses a broad colourmap window to display the full range of $T_1$.

noted, however, that this study was performed at 1.5 T. The relative merits of the different techniques may be altered at different field strengths [29].

The clinical requirements of cardiac $T_1$ mapping techniques in terms of accuracy and precision remain to be determined. Some have argued that the bias inherent in MOLLI-type techniques is unimportant, as long as the bias is consistent across patients. In this case, the improved precision offered by MOLLI would be an advantage. The reduced scan time and/or improved precision of composite IG-fitting would further enhance this advantage. Others have argued that MOLLI's sensitivity to heart rate and $T_2$ reduce the robustness of the technique – especially in patients where pathology may be present. Composite-IG fitting may partially help reduce the heart rate sensitivity; though not to the same extent as SASHA.

One limitation of the present study is that is focussed only on longer (i.e. pre-contrast) $T_1$ values. We cannot assume that the results will necessarily extend to shorter (i.e. post-contrast) $T_1$ values. In fact, the previously mentioned study by Shao et al. [23] as well as a study by Kampf et al. [30] have shown that the precision of IG fitting worsens at shorter $T_1$ values in comparison to both conventional 3-parameter as well as Bloch Equation approaches. However, note that these comparative studies employed single-IG fitting. The present study demonstrated that composite-IG provides significantly improved precision over single-IG. More significantly, these studies examined inversion groupings of the form 5(x)3. Kampf et al. [30] notes that these types of inversion groupings are suboptimal (from a precision perspective) for IG-fitting because they do not adequately sample the recovery curve for short $T_1$ values. This has also been recognized in initial work by our group [22]. As a result, we have begun to explore the use of precision-optimized inversion groupings. Initial results have shown a significant improvement in precision over a broad range of pre- and post-contrast $T_1$ values for composite-IG [22]. However, such an optimization is beyond the scope of the present work. As a result, this study focussed only on longer $T_1$ values. It will, however, be the topic of a future study. On the other hand, should the short $T_1$ precision be insufficient with a 5(x)3 acquisition, composite-IG could be incorporated into the technique of Kampf et al. [30]. They employ a conditional fitting approach which utilizes IG-fitting for high-precision and/or reduced scan time at long-$T_1$ values, and conventional 3-parameter fitting for higher precision at shorter-$T_1$ values.

## 5. Conclusions

The composite-IG fitting technique provides $T_1$ maps with high accuracy and precision for any inversion group/rest period combination. This flexibility may be used to either shorten scan time, or to achieve improved precision in equivalent scan time. In turn, this may enable a better discrimination of true pathology from artifacts and/or noise.

## Funding

This research did not receive any specific grant from funding agencies in the public, commercial, or not-for-profit sectors. It is, however, the focus of a patent filing.

## References

[1] Moon JC, Messroghli DR, Kellman P, Piechnik SK, Robson MD, Ugander M, et al. Myocardial T1 mapping and extracellular volume quantification: a Society for Cardiovascular Magnetic Resonance (SCMR) and CMR Working Group of the European Society of Cardiology consensus statement. J Cardiov Magn Reson 2013;15.

[2] Moraes GL, Higgins CB, Ordovas KG. Delayed enhancement magnetic resonance imaging in nonischemic myocardial disease. J Thorac Imaging 2013;28(2):84–95.

[3] Vermes E, Carbone L, Friedrich MG, Merchant N. Patterns of myocardial late enhancement: typical and atypical features. Arch Cardiovasc Dis 2012;105(5):300–8.

[4] Mewton N, Liu CY, Croisille P, Bluemke D, Lima JAC. Assessment of myocardial fibrosis with cardiovascular magnetic resonance. J Am Coll Cardiol 2011;57(8):891–903.
[5] Hanneman K, Nguyen ET, Thavendiranathan P, Ward R, Greiser A, Jolly MP, et al. Quantification of myocardial extracellular volume fraction with cardiac MRI in thalassemia major. Radiology 2016.
[6] Jerosch-Herold M, Sheridan DC, Kushner JD, Nauman D, Burgess D, Dutton D, et al. Cardiac magnetic resonance imaging of myocardial contrast uptake and blood flow in patients affected with idiopathic or familial dilated cardiomyopathy. Am J Physiol-Heart Circul Physiol 2008;295(3). (H1234-H42).
[7] Ugander M, Oki AJ, Hsu LY, Kellman P, Greiser A, Aletras AH, et al. Extracellular volume imaging by magnetic resonance imaging provides insights into overt and sub-clinical myocardial pathology. Eur Heart J 2012;33(10):1268–78.
[8] Liu ST, Han J, Nacif MS, Jones J, Kawel N, Kellman P, et al. Diffuse myocardial fibrosis evaluation using cardiac magnetic resonance T1 mapping: sample size considerations for clinical trials. J Cardiov Magn Reson 2012;14.
[9] Wong TC, Piehler K, Meier CG, Testa SM, Klock AM, Aneizi AA, et al. Association between extracellular matrix expansion quantified by cardiovascular magnetic resonance and short-term mortality. Circulation 2012;126(10):1206–16.
[10] Iles L, Pfluger H, Phrommintikul A, Cherayath J, Aksit P, Gupta SN, et al. Evaluation of diffuse myocardial fibrosis in heart failure with cardiac magnetic resonance contrast-enhanced T-1 mapping. J Am Coll Cardiol 2008;52(19):1574–80.
[11] Broberg CS, Chugh SS, Conklin C, Sahn DJ, Jerosch-Herold M. Quantification of diffuse myocardial fibrosis and its association with myocardial dysfunction in congenital heart disease. Circ-Cardiovasc Imaging 2010;3(6):727–34.
[12] Messroghli DR, Radjenovic A, Kozerke S, Higgins DM, Sivananthan MU, Ridgway JP. Modified Look-Locker inversion recovery (MOLLI) for high-resolution T-1 mapping of the heart. Magn Reson Med 2004;52(1):141–6.
[13] Kellman P, Herzka DA, Hansen MS. Adiabatic inversion pulses for myocardial T1 mapping. Magn Reson Med 2014;71(4):1428–34.
[14] Kellman P, Arai AE, Xue H. T1 and extracellular volume mapping in the heart: estimation of error maps and the influence of noise on precision. J Cardiov Magn Reson 2013;15.
[15] Kellman P, Hansen MS. T1-mapping in the heart: accuracy and precision. J Cardiov Magn Reson 2014;16.
[16] Sussman MS, Yang IY, Fok KH, Wintersperger BJ. Inversion group (IG) fitting: a new T-1 mapping method for modified look-locker inversion recovery (MOLLI) that allows arbitrary inversion groupings and rest periods (including no rest period). Magn Reson Med 2016;75(6):2332–40.
[17] Deichmann R, Haase A. Quantification of T1 Values by SNAPSHOT-FLASH NMR Imaging. J Magn Reson 1992;96(3):608–12.
[18] Kampf T, Reiter T, Bauer WR. An analytical model which determines the apparent T-1 for Modified Look-Locker Inversion Recovery - analysis of the longitudinal relaxation under the influence of discontinuous balanced (classical MOLLI) and spoiled gradient echo readouts. Z Med Phys 2018;28(2):150–7.
[19] Taylor JR. An Introduction to Error Analysis: The Study of Uncertainties in Physical Measurements. Mill Valley, California: University Science Books; 1982.
[20] Mulkern RV, Williams ML. The general-solution to the Bloch equation with constant RF and relaxation terms – application to saturation and slice selection. Med Phys 1993;20(1):5–13.
[21] Xue H, Shah S, Greiser A, Guetter C, Littmann A, Jolly MP, et al. Motion correction for myocardial T1 mapping using image registration with synthetic image estimation. Magn Reson Med 2012;67(6):1644–55.
[22] Sussman M. Optimized single pre/post contrast protocol for MOLLI $T_1$ mapping with inversion group (IG) fitting. Proceedings of the 25th Meeting of the International Society for Magnetic Resonance in Medicine. 2017. p. 40. Honolulu, Hawaii.
[23] Shao JX, Liu DP, Sung K, Nguyen KL, Hu P. Accuracy, precision, and reproducibility of myocardial T1 mapping: a comparison of four T1 estimation algorithms for modified look-locker inversion recovery (MOLLI). Magn Reson Med 2017;78(5):1746–56.
[24] Shao JX, Rapacchi S, Nguyen KL, Hu P. Myocardial T1 mapping at 3.0 tesla using an inversion recovery spoiled gradient echo readout and Bloch equation simulation with slice profile correction (BLESSPC) T1 estimation algorithm. J Magn Reson Imaging 2016;43(2):414–25.
[25] Roujol S, Weingartner S, Foppa M, Chow K, Kawaji K, Ngo LH, et al. Accuracy, precision, and reproducibility of four T1 mapping sequences: a head-to-head comparison of MOLLI, ShMOLLI, SASHA, and SAPPHIRE. Radiology 2014;272(3):683–9.
[26] Weingartner S, Akcakaya M, Basha T, Kissinger KV, Goddu B, Berg S, et al. Combined saturation/inversion recovery sequences for improved evaluation of scar and diffuse fibrosis in patients with arrhythmia or heart rate variability. Magn Reson Med 2014;71(3):1024–34.
[27] Chow K, Flewitt JA, Green JD, Pagano JJ, Friedrich MG, Thompson RB. Saturation recovery single-shot acquisition (SASHA) for myocardial T-1 mapping. Magn Reson Med 2014;71(6):2082–95.
[28] Piechnik SK, Ferreira VM, Dall'Armellina E, Cochlin LE, Greiser A, Neubauer S, et al. Shortened Modified Look-Locker Inversion recovery (ShMOLLI) for clinical myocardial T1-mapping at 1.5 and 3 T within a 9 heartbeat breathhold. J Cardiov Magn Reson 2010;12.
[29] Weingartner S, Messner NM, Budjan J, Lossnitzer D, Mattler U, Papavassiliu T, et al. Myocardial T-1-mapping at 3T using saturation-recovery: reference values, precision and comparison with MOLLI. J Cardiov Magn Reson 2016;18.
[30] Kampf T, Bauer WR, Reiter T. Improved post-processing strategy for MOLLI based tissue characterization allows application in patients with dyspnoe and impaired left ventricular function. Z Med Phys 2018;28(1):25–35.